ISSN: 2633-4828 Vol. 5 No.4, December, 2023

International Journal of Applied Engineering & Technology

SYNTHESIS OF 2-AMINO-4-(METHYLTHIO)BUTANOIC ACID DOPED BARIUM BROMIDE (AMB-BB) SINGLE CRYSTALS: A SEMI-ORGANIC NLO MATERIAL

Anand Kumar Pandey[1], Raghvendra Pratap Singh[1,*] and Jeet Singh[2]
[1]Department of Chemistry, Kamla Nehru Institute of Physical and Social Sciences, Sultanpur-228118, India
[2]Department of Physics, Rajkiya Mahavidyalaya, B.B. Nagar, Bulandshahr-203402, India
*E-mail: drrpsinghdrrpsingh@gmail.com

ABSTRACT
Amino acid crystals exhibit amazing nonlinear and electro-optical properties. Slow evaporation was used to create 2-amino-4-(methylthio)butanoic acid doped barium bromide, a nonlinear optical material that falls under the semiorganic category. X-ray difraction experiments on single crystals have shown that 2-amino-4-(methylthio)butanoic acid doped barium bromide (AMB-BB) is a monoclinic crystal structure. It has been demonstrated that AMB-BB contains functional groups based on FT-IR and Raman vibrational patterns. The crystal's shorter cut-off wavelength causes second harmonic generation (SHG) signals to appear at 250 nm, according to Ultra-Visible spectral analysis. Based on the UV absorption curve, 5.02eV is the optical band gap. The performance of NLO devices benefits from the determination of optical constants such as reflectance and extinction coefficient utilising UV-visible absorbance data. Non-destructive fluorescence spectroscopy is employed to examine the electrical structure of crystals that have developed. Based on its fluorescence emission spectrum, the AMB-BB crystal generates green fluorescence at an excitation wavelength of 279 nm. Its two lower intensity peaks correspond to the UV wavelength at 310 nm and the visible wavelength at 604.5 nm (orange). Additionally, the crystal displays a maximal emission peak with greatest strength at 530 nm. The mechanical and dielectric characteristics of AMB-BB were assessed by micro hardness and dielectric studies. The laser damage threshold of the synthesised crystal is measured up to 3.89 GW/cm^2, a high value compared to urea (1.50 GW/cm^2) and KDP (0.20 GW/cm^2). This implies that the crystal can be used with high-power lasers. With a Meyer's value (n) crystal of 4.50 for an AMB-BB, it is evident that the material is categorised as soft. The material's work hardening coefficient is determined by this value. Furthermore, an investigation and documentation of the dielectric behaviour as a function of frequency were conducted. Research has been observed to support the possibility of AMB-BB crystals as optical limiting devices.

Keywords: Non-linear optical, Single crystal x-ray diffraction, optical studies, Fluorescence,

Laser damaged threshold

INTRODUCTION
In order to meet the needs of contemporary applications like frequency doubling, laser remote sensing, optical switching, optical modulation, optical data storage, optical parametric oscillators (OPO), photonics, and medical diagnostics, researchers are currently looking for efficient nonlinear optical (NLO) crystals [1]. It has been demonstrated that crystal growth is of such incredible stature that it has stabilised into an amazing posture. Several nonlinear susceptibilities of the organic crystals have been observed compared to the inorganic crystals [2,3]. A multitude of findings about organic crystalline solids have been published recently [4,5], underscoring the importance of π-conjugated molecules and the structure of a three-dimensional hydrogen bonding network they generate. Amino acids are recognised to be interesting materials, especially for photonic applications, because of their chiral symmetry and non-centrosymmetric space group [6,7]. Carboxylic acids remain a class of fundamental relevance in organic compounds because they may form predictable patterns of hydrogen bonding interactions. Consequently, the topic of crystal technology has received a lot of attention lately. The available source of the amino acid synthesis process, which involves mixing carboxylic acids, has produced a plethora of accurate knowledge regarding the interactions of hydrogen bonding with reference to individual molecules [8]. Organic molecules with amine (-NH_2) and carboxyl (-COOH) functional groups, as well as a side chain (R group) unique to each amino acid, make up the crystal structure of amino acids. Carbon (C), hydrogen (H), oxygen (O), and

nitrogen (N) are the four essential constituents of an amino acid; however, some amino acids have side chains that contain other elements [9,10]. Because of their potential applications in optoelectronics, laser technology, optical storage devices, and optical communications, amino acid derivatives that also happen to be nonlinear optical (NLO) materials have attracted a lot of attention during the past 20 years [11].

Methionine is one of the twenty necessary amino acid ingredients. It is often referred to as 2-Amino-4-(methylthio)butanoic acid. It has sulphur in it, which is necessary for the normal growth and maintenance of body tissues. A number of fascinating papers on title material complexes have lately been published, and are currently available in the literature [12]. L-methionine is one of the two organic amino acids in proteins that contain sulphur, along with -Amino acid L-methionine has a protonated amino group, a deprotonated carboxylic acid group (-COO) and an S-methyl thioether side chain [13]. L-methionine functions as a precursor in the synthesis of proteins. It falls into the nonpolar and aliphatic amino acid category [14]. L-methionine and its metal derivatives are mostly known for their catalytic activity, which bestows specific antiviral properties. This amino acid is the source of creatine monohydrate, a substance needed for the synthesis of energy and the growth of muscle [15,16]. Barium bromide is the source of the chemical compounds utilised in photography and other kinds of bromides. Because radium occurs preferentially in a barium bromide solution and because the radium-to-barium ratio in the precipitate may be larger than the ratio in the solution, barium bromide was historically used in the purification of radium using Marie Curie's fractional crystallisation process [17]. A number of recently published article have reported on the complexation of L-methionine with both organic and inorganic materials, including L-phenylalanine D-methionine single crystal [18], L-methioninium picrate [19]. Consequently, amino acid complexes have received constant attention since they appear to have all the unique characteristics needed for photonics applications. The basic properties of the generated L-methionine succinic acid (LMS) single crystals are presented in this study. Methionine and cysteine are the two proteinogenic amino acids that are sulfur-containing. The crystal structures of methionine and many of its salts have been reported before [20]. Many studies are being conducted to create new organic nonlinear optical (NLO) materials because of the materials' potential applications. Maleic acid salts containing amino acids, specifically L-Alaninium maleate [22] and L-Arginine maleate [23], were recently synthesised, identified as non-limiting organic compounds, and published. In this article, a new NLO material, the molecular structure of L-methionine L-methioninium hydrogen maleate (LMMM), is reported [24].

L-Methionine or 2-amino-4-(methylthio)butanoic acid (AMBB) semi-organic material doped barium bromide (BB) single crystals are not widely explored and are now being evaluated for prospective technological purposes, according to the authors' considerable investigation and knowledge. Our objective is to create a single crystal of 2-amino-4-(methylthio)butanoic acid (AMBB) doped barium bromide (BB) and study its many mechanical, electrical, optical, structural, and physical characteristics.

2. Synthesis and crystal growth

2-Amino-4-(methylthio)butanoic acid doped barium bromide (AMB-BB) single crystals were mixed by dissolving AR grade 99% purity. Separately, dissolve barium bromide ($BaBr_2$) and 2-amino-4-(methylthio)butanoic acid ($C_5H_{11}NO_2S$) in water (solvent) at a 1:1 ratio. Stirred well and continue stirring until, after 8 hours, a homogenous solution develops at room temperature. The mixture was filtered through high-quality Whatman filter paper (grade 1) to remove any impurities. This was kept for crystal formation in a sterile beaker. The solution was then allowed to gradually evaporate at room temperature without being disturbed. Clear, colourless crystals with good definition were removed after about sixty days. The generated AMB-BB single crystals have an average size of roughly 23 mm × 7 mm × 5 mm. Fig. 1 shows an illustration of the AMB-BB crystals.

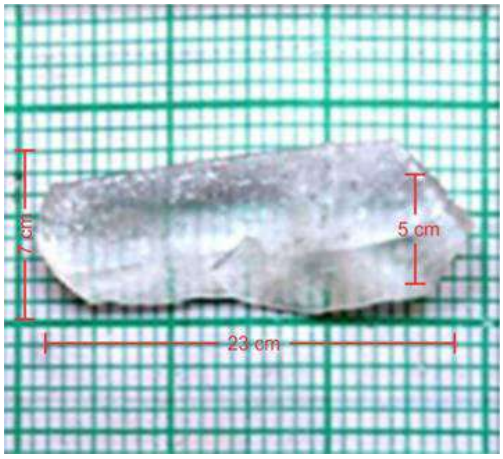

Fig.1 Pictorial representation of synthesis AMB-BB single crystals

2.1. Characterizations Techniques

The structure of AMB-BB crystals was examined using a single crystal X-ray diffractometer to ascertain the effect of barium bromide on 2-amino-4-(methylthio)butanoic acid. An ENRAF NONIUS CAD 14 Automatic X-Ray diffractometer was used to examine the X-ray diffraction of the AMB-B crystal. UV-Vis spectra in the 200–1000 nm wavelength range were obtained with a Jasco V-570 UV-VIS Spectrophotometer in order to evaluate the optical transparency of the crystals that were formed. Single crystals of AMB-BB that had been cut and polished and had a thickness of around 2 mm were used for the current experimental investigations. The room temperature fluorescence emission spectra of LMBB were obtained with a Perkin-Elmer LS 45 spectrophotometer. FT-IR and FT-Raman spectra were used to identify the presence of several functional groups. Using an IRAffinity-1 CE, FTIR spectra were obtained in the 4000–400 cm^{-1} range to look at the coordination of metal complexes (Shimadzu Corporation analytical and measuring equipment division, Kyoto, Japan). The FT-Raman spectra of the formed crystals were obtained at 4 cm^{-1} resolution in the 4500-400 cm^{-1} range using a Perkin-Elmer GX 2000. A 20 ns pulse width Nd-YAG Q-Switched laser was used. Multiple-shot LDT measurements were performed in the well-polished crystal. The sample was exposed to a 1 mm spot size of the regulated laser light, and the energy output was measured. The laser light intensity was modified and applied to the sample using the variable attenuator. During laser irradiation, it was observed that the laser beam possessed a high energy. Thus, Vickers micro-indentations hardness tests were performed using Leitze Wetzlar hardness testers equipped with square diamond indenters. A variety of loads ranging from 10 to 100 g were utilised in order to ascertain the microhardness value (H_v). The dielectric was measured using an Agilent 4284A precision LCR metre set to oscillate at 1 V amplitude. The dc electrical resistivity samples were measured at room temperature up to 100 °C in a constant electric field of 60 V/cm using a Keithley 6517A programmable electrometer.

3. RESULTS AND DISCUSSION

3.1. Single XRD studies

An analytical technique for identifying atom configurations inside a crystalline sample is single X-ray diffraction. For AMB-BB crystal, single XRD is used to determine the properties of the unit cell and the three-dimensional coordinates of the atoms inside it [25]. The lattice parameters of the crystal are as follows: a = 10.47 Å, b = 7.93 Å, c = 8.96 Å, α = γ = 90º, β = 113.53º, V(Å) The result for 3 is 645, which suggests that it belongs to the monoclinic system and that its *C*2/*c* space group, as shown in Table-1, is consistent with values that have been previously published [26].

Table-1 Lattice parameters of AMB-BB crystals

Sample	Lattice Parameters (Å)			Volume ($Å^3$)
	a (Å)	b (Å)	c (Å)	V
Reported work [Ref. 3]	10.74	7.39	8.69	633
Present work	10.47	7.69	8.86	614.86

3.2. OPTICAL STUDIES

3.2.1. UV-Vis analysis

Important information regarding the electrical properties, chemical structure, and electronic resonance structure can be found in the UV-Vis and NIR light spectra. When electrons undergo ground state transitions, they absorb UV-VIS light, which is generated upon electron stimulation. For optical device applications, large transmittance ranges and low cutoff wavelengths are required [28,29]. Since it is essential to their use, nonlinear optical materials cannot function without a wide transparency window.[30].

It has been demonstrated that AMB-BB crystal has higher optical transparency (over 90%) in the visible spectrum, which makes it a promising material for nonlinear optics. The absorbance spectra displayed in Fig.2a indicated that the cut-off wavelength for AMB-UV BB was 250 nm. The observed UV-visible absorption spectra show no appreciable absorption in the visible NIR and IR regions. Because the crystal exhibits remarkable transmittance throughout the visible spectrum, these optical materials with a nearly perfect transmittance window in the visible domain are perfect for non-linear optical applications [31]. The optical band energy of the produced $^{1/2}$ *versus* Tauc's relation. Additionally, the bandgap can be computed using the eqn. 1:

$$E_g = 1240/\lambda_{onset} \quad (1)$$

where E_g denotes the bandgap energy and onset denotes the absorption edge as determined by the absorption spectra. The outcomes of the previously given formula matched the Tauc relation curves quite well [32]. A large range of band gaps in the title compound cause it to exhibit enormous transmittance in the visible spectrum [33]. The absence of energy absorption across the visible spectrum indicates that the generated AMB-BB is a favourable material in the field of nonlinear second harmonic creation. [34].

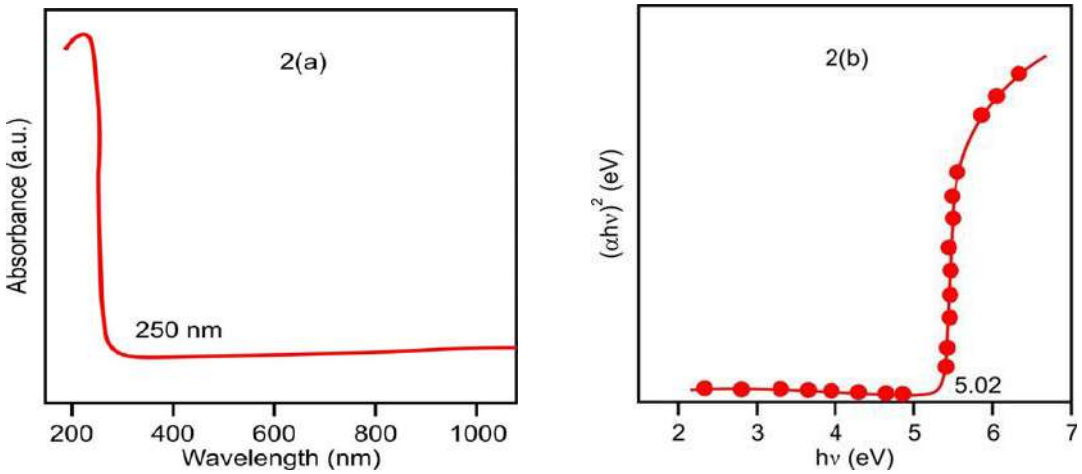

Fig.2. UV-spectroscopy spectra (a) Absorbance curve and (b) band gap

3.2.2. Optical Constant determination

The way materials are employed in optoelectronic devices is largely determined by their optical characteristics. There may be a high correlation between a material's optical properties and its electrical properties, electronic band structure, and atomic structure [35]. It is easy and accurate to measure the optical constant with inorganic crystals. It is possible to accurately control the optical density of states and the spatial distribution of the photonic mode in such crystals. Figs. 2c and 2d, which show the variation of reflectance (R) and extinction coefficient (k) as a function of absorption coefficient, respectively, clearly demonstrate that both reflectance and extinction coefficient depend linearly on photon energy [36]. The internal efficiency of the device is also impacted by the absorption coefficient. Optoelectronic devices can be produced if the proper material is obtained [37,38]. The following illustrates how the extinction coefficient (K) and reflectance (R), which are connected to the absorption coefficient (α), are displayed. The absorption coefficient affects the device's internal efficiency as well. By achieving the right material, optoelectronic devices can be made [37,38]. The extinction coefficient (K) and reflectance (R), which are related to the absorption coefficient (α), can be shown in the following eqns. 3 and 4 [36]:

$$K = \alpha\lambda/4\pi \qquad (3)$$

$$R = 1 \pm \sqrt{1-\exp(-\alpha t)} + (\alpha t)/1 + \exp(-\alpha t) \qquad (4)$$

Figs. 2c and 2d show how reflectance (R) and extinction coefficient (K) fluctuate with photon energy hυ. It is anticipated that the AMB-BB crystal's high transmittance will be a consequence of its low extinction coefficient and reflectance. This has incredible applications in nonlinear optics.

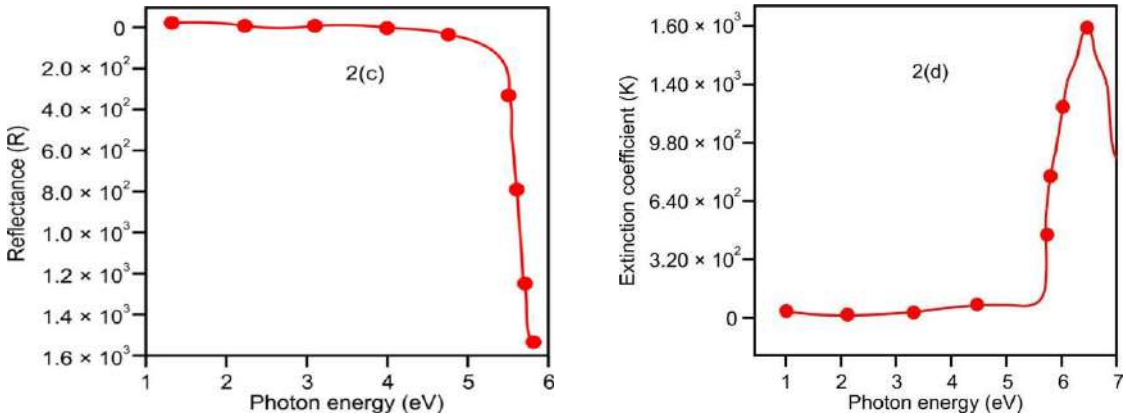

Fig.2. Determination of optical constant (c) reflectance and (d) extinction coefficients

3.3. Fluorescence studies

Fluorescence (FL) spectroscopy is a non-destructive, contactless technique for analysing a material's electrical structure. It is the material's optically stimulated, naturally occurring light release. Aromatic compounds feature several conjugated double bonds that are remarkably stable at resonance, which is a physicochemical property [39]. To verify the emission spectrum associated with this particular excited state, measurement of the fluorescence spectra for the AMB-BB crystal were made. The AMB-BB wide emission spectra were measured between 200 and 1000 nm, which is the excitation wavelength range. Fig.3 displays the fluorescence emission spectra of the AMB-BB crystal at 279 nm excitation wavelengths. In the FL spectrum, there were two additional peaks that were less intense. This is equal to an ultraviolet wavelength of 310 nm and 604.5 nm (orange). At 530 nm, the crystal's intensity reaches its maximum emission peak, indicating that green fluorescence is being emitted. Furthermore, a solitary, acute peak indicates excellent crystalline perfection [40].

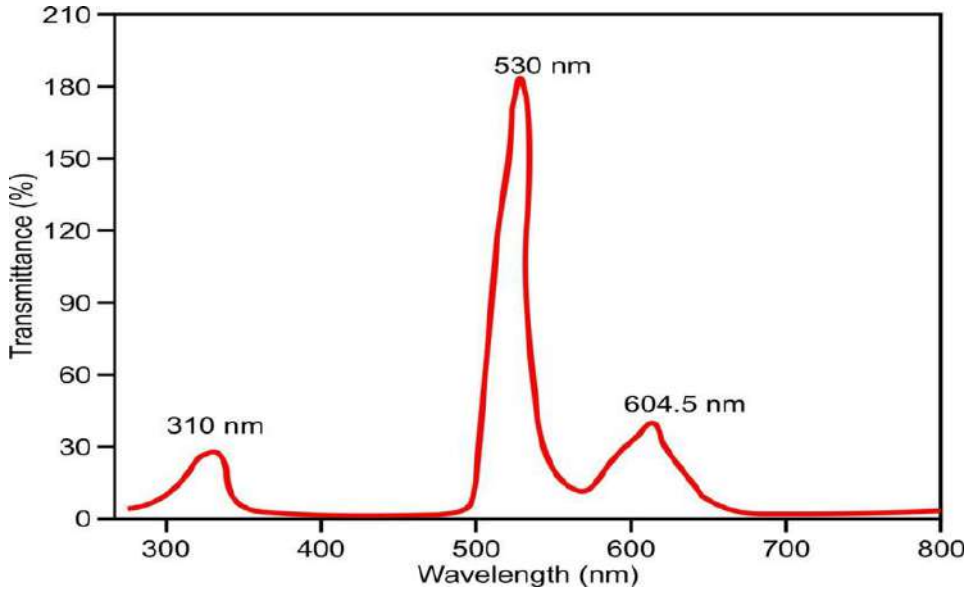

Fig.3. Fluorescence spectrum of AMB-BB single crystal

3.4. FT - Raman spectral studies of AMB-BB

Fig. 4 is illustrated by the spectroscopic pictures of AMB-BB crystals. In Raman absorption, NH_3^+ asymmetric stretching peaks at 3390 cm [41]. In Raman spectrum, a C–C stretching vibration occurs at 1616 cm . The Raman spectrum shows the appearance of the C-C stretching modes at 717 cm . The Raman frequencies 595 and 440 cm correspond to C–C–C out of plane bending and C–C–C out of ring deformation, respectively [42].

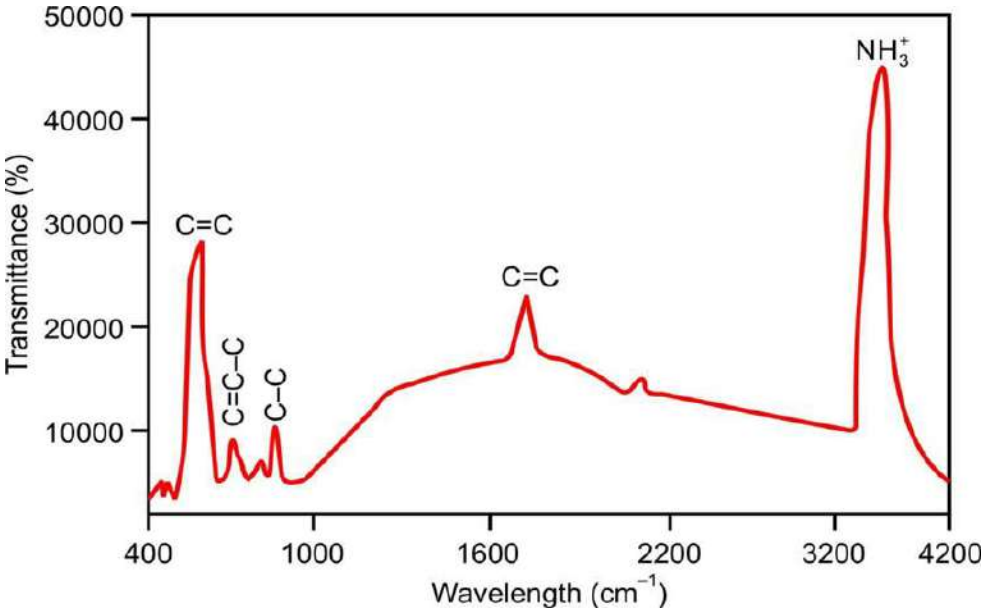

Fig.4. FT-Raman spectrum of AMB-BB single crystal

3.5. FT-IR Vibrational spectroscopy

In the infrared, the absorption peaks are NH_3^+ asymmetric stretching at 3390 cm . The medium broad band at 2918 cm in the infrared showed that CH_3 asymmetric stretching was present [43]. The peak at IR at 2621 cm is caused by the symmetric stretching mode of NH_3^+ [44]. The NH_3^+ symmetric deformation is confirmed by the

infrared signal at 1519 cm . The C–C stretching vibration is observed at 1602 cm in the infrared range [45], whereas the COO-weak band has an absorption band visible at 1420 cm in the infrared spectrum [46]. The C-COO stretching vibration at 1282 cm and the CH_2 twisting vibration at 1241 cm in the infrared spectrum are caused by the rocking of NH_3^+ vibration [43]. The IR spectra show the C-C stretching modes at 740 cm .

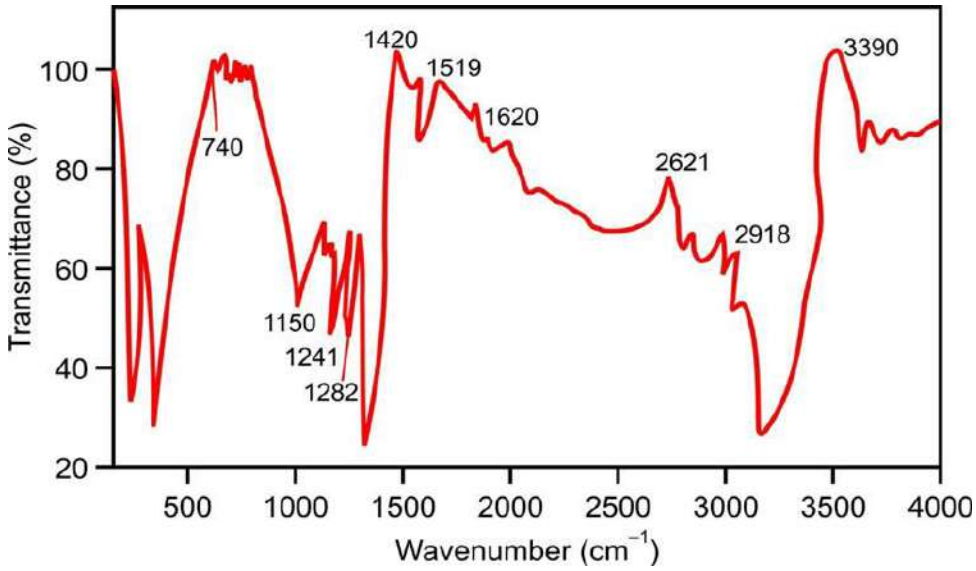

Fig.5. FT-IR Vibrational spectrum of AMB-BB single crystal

3.6. Surface laser damage threshold (LDT) studies

Surface laser damage to nonlinear optical materials is caused by non-linear optical processes that are impacted by high light intensity. The NLO materials must sustain despite the high power intensities [47]. This formula was used to determine AMB-laser BB's damage threshold.

$$Pd = E/\tau A \qquad (5)$$

where τ is the pulse width (ns), A is the circular spot size area, and E is the pulse energy (mJ/ cm^2). According to this study, surface laser damage from the AMB-BB crystal may be 3.89 GW/cm^2. Because of its higher value as compared to urea (1.50 GW/cm^2) and KDP (0.20 GW/cm^2), high-power lasers can be utilised with it [31]. Growing crystal demonstrates a lower laser damage threshold (5.71 GW/cm^2) for L-methionine DL-mandelic acid in comparison to previous studies [48]. This study demonstrates that due to its metal complexes, when BaBr replaces K (potassium), the corresponding laser damage threshold value is much lower.[49].

3.7. Microhardness studies

The structure and chemical composition of crystals have a major impact on their mechanical properties. The following expression (6) has been used to calculate the micro-hardness values for the AMB-BB single crystal at each load:

$$H_v = 1{\cdot}8544 \times P/d^2 \ (Kg/mm^2) \qquad (6)$$

where P is the applied force in grammes, d is the diagonal length of the indentation mark in microns, and H_v is represented in kg mm^2. The relationship between the Vickers hardness number and applied load P is seen in Fig. 6a. Plotting against the hardness number (H_v) and applied load (P) is displayed in Fig. 6a's curve [50-52]. As the applied force increases, the hardness number (H_v) in the AMB-BB crystal rises due to the reverse indentation size effect (RISE) (P) [46].

The load variation can be interpreted by using Meyer's law equation (7),

$P = K_1 dn$ (7)

where P is the applied force, d is the diagonal length of the impression, K_1 is a constant, and n is the Meyer's index, also known as the work hardening coefficient. The slope of In P *versus* In d (Fig. 6) yields the value of n. The work hardening coefficient of an AMB-BB, which is 4.50 according to Meyer's value (n) crystal, makes it abundantly evident that the material is soft [53]. Therefore, in order to create devices, it is important to increase the mechanical strength of the crystal. AMB-BB crystal's hardness and sufficient mechanical strength allow it to be utilised to create a range of NLO devices.

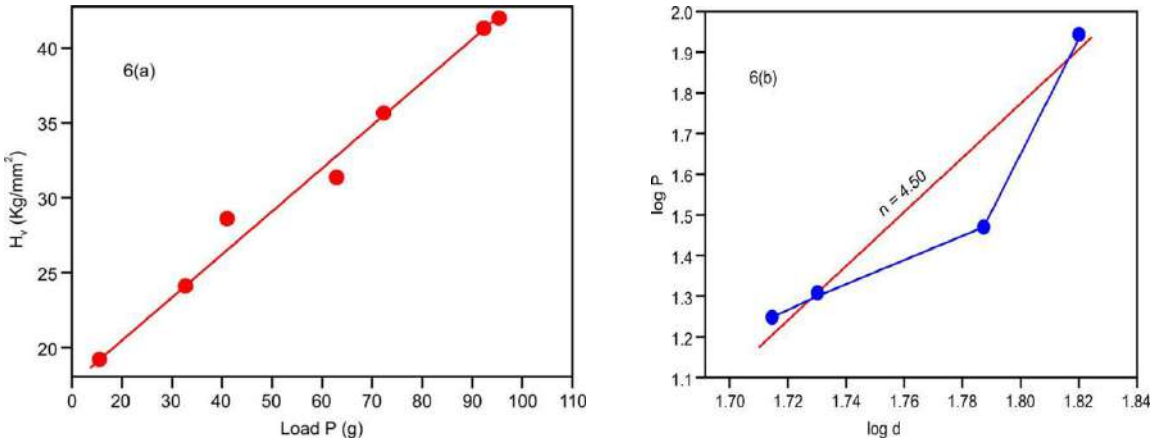

Fig.6. (a) Variation of hardness number *versus* load applied P for AMB-BB and (b) Meyer's plot for AMB-BB crystal.

3.8. Dielectric studies

The dielectric properties of optical materials are intimately associated with the electro-optic properties of non-conducting crystals. A sample with a silver coating on the opposite faces and dimensions of (4 × 2 × 1) mm on each side is used to measure the dielectric. The dielectric constant (
frequency, from 1.0 Hz to 5.5 MHz, are shown in Fig. 7a and 7b, respectively.

When the frequency is raised from 1.5 to 5.0, the dielectric constants show a drop in Fig. 7a of the samples that does not change. The crystal structure, electronic polarizability, and atomic polarizability of a crystal determine its dielectric behaviour at low frequencies (eqn. 8 and 9) [54]:

$\varepsilon' = Cd/A\varepsilon_0$ (8)

$\varepsilon'' = \varepsilon' \tan \delta$ (9)

The symbol d in this expression stands for the crystal thickness. A is an area represented by capacitance, and ε is the vacuum's dielectric constant. the relationship in which the dissipation factor D was used to compute the crystal's dielectric loss.

Figs. 7a and 7b show how frequency affects the dielectric constant and dielectric loss of the produced crystal. The dielectric constant falls until it approaches a constant value in frequency-dependent dielectric constants and dielectric losses. Therefore, space charges, which exist in the structure as defects like oxygen vacancies, can be responsible for the larger dielectric constant values at lower frequencies. Low dielectric constant values are the result of space charge polarisation saturation at higher frequencies. All of the samples show a drop in dielectric constant with increasing frequency, and at 100 kHz, the contribution from space charge polarisation is seen. Greater frequencies result in lower dielectric constant values because dipoles are unable to follow the quickly

changing field, whereas lower frequencies result in higher dielectric constant values because dipoles can follow the alternating field. The current data agrees well with the previously published [55].

The grown crystal has extremely minimal loss over the complete range of the designated frequencies, as seen clearly in Fig. 7b, indicating that there are no structural defects in the single crystal. As frequency rises, the dielectric loss decreases. The increased dielectric loss at lower frequencies can be explained by oxygen vacancies, which act as space charges and whose contribution is dominant at lower frequencies. For many NLO materials and their applications, this feature, which shows negligible dielectric loss at a high frequency is especially important [56].

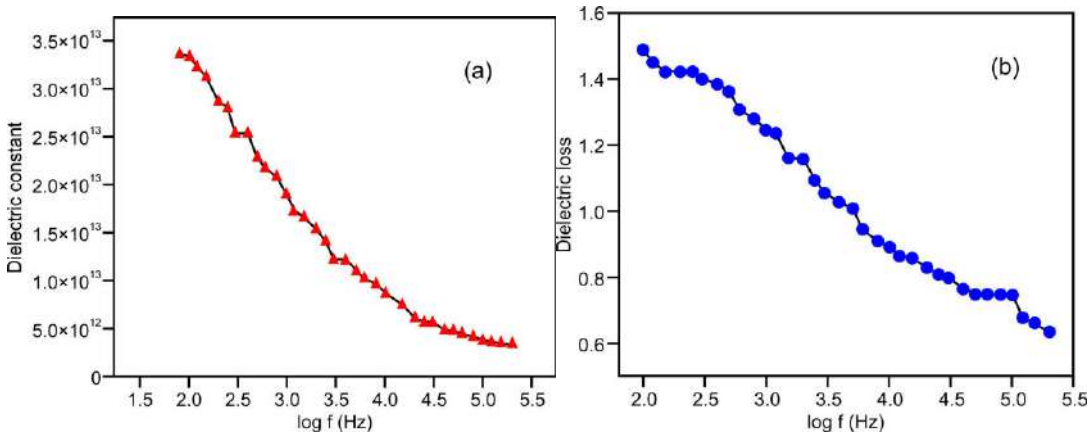

Fig. 7 (a) Dielectric constant Vs log frequency and (b) Dielectric loss Vs log frequency for AMB-BB single crystal

4. CONCLUSION

The slow evaporation solution growth method was used to generate the semi-organic single crystal of 2-amino-4-(methylthio)butanoic acid doped barium bromide (AMB-BB). The AMB-BB crystal structure had been established using single-crystal X-ray diffraction. AMB-BB crystallised in a monoclinic system belonging to the space group *C*2/*c*. FT-IR and FT-Raman spectral data analysis reveals multiple functional groups. Using UV-Vis-NIR optical experiments, the lowest cut-off wavelength of the crystal, which is 250 nm, was determined. and ascertained the optical band gap, determining it to be 5.02 eV. Optical constants like reflectance (R) and extinction coefficient (K) were assessed based on the photon energy. The reverse indentation size effects of the crystal are confirmed by microhardness measurements. The dielectric loss and dielectric constant of the crystal are investigated at various frequencies. It shows green fluorescence emission, as indicated by the measured emission peak at 520 nm, which corresponds to the maximum intensity of the crystals. Additionally, a single, sharp peak denoting good crystalline perfection is seen. The AMB-BB single-shot laser damage threshold with the Nd: YAG laser at 1064 nm wavelength is 3.98 GW/cm^2.Thus, AMB-BB single crystals seems to be an appropriate candidates for optical limiting applications.

REFERENCES

1. S. Janet Priyavathani, S. Stella Mary, S. Sahaya Jude Dhas, P. Gandhimathi and S. Usharani, Chemical Physics Impact, 6, June 2023, 100203. https://doi.org/10.1016/j.chphi.2023.100203
2. I.R. Zachea, Ya. Shchur, R.R. Levitskii, A.S. Vdovych;, Thermodynamic properties of ferroelectric NH3CH2COOH·H2PO3 crystal, Physica B 520 (2017) 164–173.
3. K. Sethuraman, R. Ramesh Babu, R. Gopalakrishnan, P. Ramasamy;, Unidirectional growth of (110) ammonium dihydrogen orthophosphate single crystal by Sankaranarayanan–Ramasamy method, J. Cryst.Growth 294 (2006) 349–352.

4. S.R. Maidur, J.R. Jahagirdar, P.S. Patil, T.S. Chia, C.K. Quah, Structural Characterizations, Hirshfeld surface analyses, and third-order nonlinear optical properties of two novel chalcone derivatives, Opt. Mater. 75 (2018) 580–594 (Amst).

5. M.K. Kumar, S. Sudhahar, P. Pandi, G. Bhagavannarayana, R.M. Kumar, 476 studies of the structural and third-order nonlinear optical properties of solution grown 4- 477 hydroxy-3-methoxy-4′-N′-methylstilbazolium tosylate monohydrate crystals, Opt. Mater. 478 (36) (2014) 988–995.

6. A. Sivakumar, S. Sahaya Jude Dhas, P. Sivaprakash, R.S. Kumar, S. Arumugam, S. A. Martin Britto Dhas, Structural and morphological behaviours of L-Asparagine monohydrate at shocked conditions, Physica B 651 (2023), 414580.

7. A. Sivakumar, S. Sahaya Jude Dhas, P. Sivaprakash, S. Prabhu, K. Moovendaran, A. Murugeswari, S. Arumugam, S.A. Martin Britto Dhas, Shock wave induced conformational phase transition of L-leucine, J. Mole. Struct. 1271 (2022), 134033.

8. A. Sivakumar, S. Sahaya Jude Dhas, J. Thirupathy, P. Sivaprakash, K. Anitha, R.S. Kumar, S. Arumugam, S.A. Martin Britto Dhas, Investigation on crystallinity and optical properties of L-tartaric acid single crystal at dynamic shocked conditions,J. Mater. Sci. Mater. Electron. (2022), https://doi.org/10.1007/s10854-022-08065-4.

9. L. Cao, B. Teng, K. Feng, D. Zhong, L. Hao, Q. Sun, Growth and defects of DAST crystal in high concentration solution, J. Cryst. Growth 412 (2015) 20–24.

10. T. Tian, B. Cai, T. Ye, Q.Q. Cheng, P. Zhan, G. Xu, L. Zhanga, O. Sugihara;, Oneminute self-assembly of millimetre-long DAST crystalline microbelts via substratesupported rapid evaporation crystallization, RSC Adv. 7 (2017) 31691.

11. Amino acids-precursors for synthesizing nonlinear optical materials, Progress in Crystal Growth and Characterization of Materials. Volume 58, Issues 2–3, June–September 2012, Pages 74-83. https://doi.org/10.1016/j.pcrysgrow.2012.03.002.

12. Becquet P, Vazquez-Anon M, Mercier Y, Wedekind K, Mahmood T, Batonon-Alavo DI, Yan F. A systematic review of metabolism of methionine sources in animals: One parameter does not convey a comprehensive story. Anim Nutr. 2023 Jan 24;13:31-49. doi: 10.1016/j.aninu.2023.01.009.

13. Development of coordination chemistry with thiol-containing amino acids, Nobuto Yoshinari, Naoto Kuwamura, Tatsuhiro Kojima, Takumi Konno, Coordination Chemistry Reviews, Volume 474, 1 January 2023, 214857. https://doi.org/10.1016/j.ccr.2022.214857.

14. Growth and characterization of L - Methionine Barium Bromide (LMBB) semi-organic crystal for optical limiting applications, M. Shalini [a], R.S. Sundararajan [a b], E. Manikandan [c], M. Meena [a b], B. Samuel Ebinezer [a b], T.C. Sabari Girisun [d], R. Natarajan , Optik, Volume 278, May 2023, 170705.https://doi.org/10.1016/j.ijleo.2023.170705

15. da Silva RP, Nissim I, Brosnan ME, Brosnan JT. Creatine synthesis: hepatic metabolism of guanidinoacetate and creatine in the rat in vitro and in vivo. Am J Physiol Endocrinol Metab. 2009 Feb;296(2):E256-61. doi: 10.1152/ajpendo.90547.2008.

16. Synthesis and structure–activity relationship of L-methionine-coupled 1,3,4-thiadiazole derivatives with activity against influenza virus, Esra Tatar, Seda Yaldız, Necla Kulabaş, Evelien Vanderlinden, Lieve Naesens, İlkay Küçükgüzel, Chemical Biology and drug design, Volume99, Issue3, March 2022,Pages 398-415. https://doi.org/10.1111/cbdd.13995.

17. Ruth Lewin Sime Lise Meitner: A life in physics Univ of California Press, (1996)

18. P. Sangeetha, P. Jayaprakash, M. Nageshwari, C. Rathika Thaya Kumari, S. Sudha, M. Prakash, G. Vinitha, M. Lydia Caroline, Growth and characterization of an efficient new NLO single crystal L-phenylalanine D-methionine for frequency conversion and optoelectronic applications, Phys. B Condens. Matter 525 (2017) 164–174, https://doi.org/10.1016/j.physb.2017.08.037.

19. V.V. Ghazaryan, B.A. Zakharov, E.V. Boldyreva, A.M. Petrosyan, L-Methioninium picrate, Spectrochim. Acta Part A Mol. Biomol. Spectrosc. 142 (2015)344–349, https://doi.org/10.1016/j.saa.2015.02.036

20. Structural, optical, magnetic and thermal properties of L-methionine succinic acid single crystal for photonic applications,S. Janet Priyavathani, S. Stella Mary, S. Sahaya Jude Dhas, P. Gandhimathi, S. Usharani, Chemical Physics Impact, Volume 6, June 2023, 100203. https://doi.org/10.1016/j.chphi.2023.100203.

21. Natarajan S, Martin Britto S A. and Ramachandran E. Cryst. Growth Des. 2006;6:137. doi: 10.1021/cg0502439.

22. Mallik T, Kar T, Bocelli G. and Musatti A. Sci. Technol. Adv. Mater. 2005;6:508. doi: 10.1016/j.stam.2005.01.001.

23. Ramaswamy S, Sridhar B, Ramakrishnan V and Rajaram R K. 2004. Acta Cryst.E 60 01691.

24. Natarajan S, Rajan Devi N, Britto Dhas SD, Athimoolam S. Crystal growth and structure of L-methionine L-methioninium hydrogen maleate-a new NLO material. Sci Technol Adv Mater. 2008 Jul 10;9(2):025012. doi: 10.1088/1468-6996/9/2/025012.

25. Koteeswari Pandurangan, Sagadevan Suresh, Synthesis, growth, and characterization of bisglycine hydrobromide single crystal,J. Mater., 2014 (2014), 10.1155/2014/362678.

26. Growth and characterization of L - Methionine Barium Bromide (LMBB) semi-organic crystal for optical limiting applications. M. Shalini, R.S. Sundararajan. Manikandan, M. Meena. Samuel Ebinezer, T.C. Sabari Girisun, R. Natarajan, Optik, Volume 278, May 2023, 170705. https://doi.org/10.1016/j.ijleo.2023.170705.

27. B. Helina, P. Selvarajan, A.S.J. Lucia Rose, Structural, optical, thermal, Mechanical and electrical characterizations of γ-glycine crystals grown in strontium chloride solution. Phys. Scr., 5 (2012), Article 055803, 10.1088/0031-8949/85/05/055803.

28. K. Nivetha, S. Kalainathan, M. Yamada, Y. Kondo, F. Hamada

29. Synthesis, growth, and characterization of new stilbazolium derivative single crystal: 2-[2-(2, 4-dimethoxy-phenyl)-vinyl]-1-ethyl-pyridinium iodide for third-order NLO applications. J. Mater. Sci.: Mater. Electron., 28 (7) (2017), pp. 5180-5191, 10.1007/s10854-016-6174-x.

30. Advances in aliovalent substitution strategy for the design and synthesis of nonlinear optical materials: d0 transition metal/gallium iodates and selenites. Coordination Chemistry Reviews

Volume 490, 1 September 2023, 215212. https://doi.org/10.1016/j.ccr.2023.215212.

31. Liu, TM., Conde, J., Lipiński, T. et al. Revisiting the classification of NIR-absorbing/emitting nanomaterials for in vivo bioapplications. NPG Asia Mater 8, e295 (2016). https://doi.org/10.1038/am.2016.106.

32. Enhanced photocatalytic degradation of Acid Blue dye using CdS/TiO2 nanocomposite. Nida Qutub, Preeti Singh, Suhail Sabir, Suresh Sagadevan & Won-Chun Oh, Scientific Reports, (2022) 12:5759 | https://doi.org/10.1038/s41598-022-09479-0.

33. Wang P, Chu Y, Tudi A, Xie C, Yang Z, Pan S, Li J. The Combination of Structure Prediction and Experiment for the Exploration of Alkali-Earth Metal-Contained Chalcopyrite-Like IR Nonlinear Optical Material. Adv Sci (Weinh). 2022 May;9(15):e2106120. doi: 10.1002/advs.202106120.

34. Investigation on crystal growth, spectral, linear optical studies, and third-order nonlinear optical analysis of L-Cysteine hydrochloride monohydrate lithium sulphate (L-CHMLS) single crystals for optical limiting applications, M. Meena, M. Shalini, B. Samuel Ebinezer, R. S. Sundararajan, T. C. Sabari Girisun , and E. Manikandan, J Mater Sci: Mater Electron (2023) 34:1778. https://doi.org/10.1007/s10854-023-11195-y.

35. III-V compound SC for optoelectronic devices, lSudha Mokkapati, Chennupati Jagadish, Materials Today, Volume 12, Issue 4, April 2009, Pages 22-32. https://doi.org/10.1016/S1369-7021(09)70110-5.

36. Growth, theoretical and optical studies on potassium dihydrogen phosphate(KDP) single crystals by modified Sankaranarayanan–Ramasamy(mSR) method, R. Robert, C. Justin Raj, S. Krishnan, S. Jerome Das, Physica B 405 (2010) 20–24, doi:10.1016/j.physb.2009.08.015.

37. V. Pandey, N. Mehta, S.K. Tripathi, A. Kumar, Chalcogenide Lett. 2 (2005) 39.

38. M. Dongol, Egypt. J. Solids 25 (2002) 33.

39. Markus SauerJohan HofkensJohan HofkensJörg EnderleinJörg Enderlein , Handbook of Fluorescence Spectroscopy and Imaging: From Single Molecules to Ensembles, February 2011. DOI: 10.1002/9783527633500.

40. V. Mohanraj, M. Thenmozhi, R. Pavithra, J. Jaslin, A. Christopher, S. Jebamalar, R. Umarani, Growth, structure, spectral characterization, fluorescence and thermal studies on phenyltrimethylammonium trichloro cadmiate (II) crystals. J. Environ. Nanotechnol., 9 (1) (2021), pp. 42-49, 10.13074/jent.2020.03.201399.

41. M. Prabhakaran, C. Karnan, S. Manivannan, S. Azhagiri, Crystal growth, optical, thermal, mechanical and laser damage threshold properties of nonlinear optical l-methionine inserted potassium pentaborate (LMKB5) single crystal for optoelectronic applications. J. Electron. Mater., 50 (8) (2021), pp. 4388-4396, 10.1007/s11664-021-08972-y

42. K. Uthayarani, R. Sankar, C.K. Shashidharan Nair. Growth, spectral and thermal properties of KAP single crystals in the presence of DL-Alanine and L-Methionine amino acid dopants. Cryst. Res. Technol. J. Exp. Ind. Crystallogr., 43 (7) (2008), pp. 733-739, 10.1002/crat.200711091.

43. V.C. Vincent, G. Bakiyaraj, K. Kirubavathi, K. Selvaraju, Synthesis, growth, and theoretical investigations of L-methionine L-methioninium perchlorate monohydrate a nonlinear optical crystal, Chem. Data Collect., 22 (2019), Article 100247, 10.1016/J.CDC.2019.100247.

44. M. Nageshwari, C. Rathika Thaya Kumari, G. Vinitha, M. Peer Mohamed, S. Sudha, M. Lydia Caroline, Crystal growth, structural, spectral, thermal, dielectric, linear and nonlinear optical characteristics of a new organic acentric material: l-Methionine-Succinic acid (2/1) J. Mol. Struct., 1155 (2018), pp. 101-109, 10.1016/j.molstruc.2017.10.099

45. V.V. Ghazaryan, B.A. Zakharov, E.V. Boldyreva, A.M. Petrosyan L-Methioninium picrate Spectrochim. Acta Part A Mol. Biomol. Spectrosc., 142 (2015), pp. 344-349, 10.1016/j.saa.2015.02.036.

46. P. Jayaprakash, P. Sangeetha, C. Rathika Thaya Kumari, M. Lydia Caroline, Investigation on the growth, spectral, lifetime, mechanical analysis and third-order nonlinear optical studies of L-methionine admixtured D-mandelic acid single crystal: a promising material for nonlinear optical applications, Phys. B Condens. Matter, 518 (2017), pp. 1-12, 10.1016/j.physb.2017.05.017

47. D ARIVUOLI , Fundamentals of nonlinear optical materials, Pramana – J. Phys., Vol. 57, Nos 5 & 6, Nov. https://www.ias.ac.in/article/fulltext/pram/057/05-06/0871-0883.

48. P. Jayaprakash, P. Sangeetha, C. Rathika Thaya Kumari, M. Lydia Caroline, Investigation on the growth, spectral, lifetime, mechanical analysis and third-order nonlinear optical studies of L-methionine admixtured

D-mandelic acid single crystal: a promising material for nonlinear optical applications. Physica B 518, 1–12 (2017)].

49. Chen Y, Gao H, Wang X, Guo D, Liu Z. Laser Induced Damage of Potassium Dihydrogen Phosphate (KDP) Optical Crystal Machined by Water Dissolution Ultra-Precision Polishing Method. Materials (Basel). 2018 Mar 13;11(3):419. doi: 10.3390/ma11030419.
50. E.M. Onitsch, Microscopia, 2 (1947), pp. 131-151
51. M. Hanneman, Metall. Manch., 23 (1941), pp. 135-140
52. C.B. Ponton, R.D. Rawling Br. Ceram. Trans. J., 88 (1989), p. 83.
53. Enhancement of electro-optic and structural properties of TGS single crystals on doping with l-glutamic acid. Preeti Singh, M. M. Abdullah, Suresh Sagadevan, Saiqa Ikram, Journal of Materials Science: Materials in Electronics (2018) 29:7904–7916. https://doi.org/10.1007/s10854-018-8790-0.
54. Observation of crystallization and characterizations on thiourea cadmium iodide: A semi-organic optical material, Preeti Singh, Mohd. Hasmuddin, M.M. Abdullah, Mohd. Shkir, M.A. Wahab, Materials Research Bulletin 48 (2013) 3926–3933.http://dx.doi.org/10.1016/j.materresbull.2013.06.005.
55. Investigation on structural, optical, thermal, mechanical and dielectric properties of L-proline cadmium chloride monohydrate single crystals:An efficient NLO material, Preeti Singh a, Mohd. Hasmuddin a, Mohd. Shakir a,b,e, N. Vijayand, M.M. Abdullah, V. Ganesh d, M.A. Wahab, Materials Chemistry and Physics 142 (2013) 154e164. http://dx.doi.org/10.1016/j.matchemphys.2013.06.051.
56. M. Anis, G.G. Muley, Influence of tartaric acid on linear-nonlinear optical and electrical properties of KH2PO4 crystal, J. Opt. Mater., 72 (2017), pp. 1-7, 10.1016/j.optmat.2017.05.04